Kinetics Study and Crystallization Process Design for Scale-Up of UiO-66-NH_2 Synthesis

Paul M. Schoenecker, Grace A. Belancik, Bogna E. Grabicka, and Krista S. Walton
School of Chemical and Biomolecular Engineering, Georgia Institute of Technology, Atlanta, GA 30332

DOI 10.1002/aic.13901
Published online August 30, 2012 in Wiley Online Library (wileyonlinelibrary.com).

A comprehensive scale-up procedure for amine-functionalized UiO-66 is implemented, which leads to the development of a novel flow-through metal-organic framework synthesis process. Products are characterized via BET modeling of N_2 adsorption at 77 K and powder XRD to confirm crystal porosity and phase, respectively. Batch syntheses are conducted to examine the effects of polytetrafluoroethylene and glass vessel materials on crystal yield and quality. Intermediate samples from sealed-vessel trials at 373, 383, and 393 K are collected and characterized, which show a high degree of product consistency. Nucleation rates are determined at the same temperatures, and the Arrhenius relationship is used to predict the activation energy of nucleation, E_{aNuc}. A continuous-flow reactive crystallization process is developed using a draft-tube type reactor. As a proof of concept, the reactor is operated for three retention times. The cumulative product, material retained within the crystallizer, and intermediate samples are collected and characterized to confirm UiO-66-NH_2 production. © 2012 American Institute of Chemical Engineers *AIChE J,* 59: 1255–1262, 2013
Keywords: metal-organic framework, crystallization, kinetics, process, adsorption

Introduction

Metal-organic framework (MOF) synthesis and characterization have increased exponentially in recent years. As a family of porous-crystalline materials, MOFs provide a multitude of pore geometries, connectivities, and chemical functionalities that can be further tuned by postsynthetic modification (PSM). Due in part to the nearly infinite structure possibilities, MOFs exhibit potential for a plethora of applications including gas separation and storage,[1–5] catalysis,[6,7] drug delivery,[8–10] and thin film applications.[11,12] Amine-functionalized MOFs including IRMOF-3, DMOF-1-NH_2, and UiO-66-NH_2 are of particular importance for many applications. The amine-functionality proves beneficial for selective gas adsorption[13] and NO delivery[14] as well as facilitating PSM via anhydride substitution.[15,16]

The reported water sensitivity of certain MOFs[17–20] and the subsequent concern that MOF performance tends to decrease under humid conditions has hindered the transition of these materials to an applied level. However, recent reports have emerged of materials capable of withstanding water exposure, including nitrogen-coordinated and highly coordinated MOFs.[13,21–23] In addition to a high degree of water stability, the amine-functionalized analog of UiO-66 is expected to exhibit a similar degree of chemical and mechanical stability reported for the parent material.[24] This will be highly advantageous not only for harsh environment applications but filtration applications in general, where the ability to press pellets of materials with minimal or no binder required can significantly reduce the pressure drop across the filter without sacrificing adsorption capacity.

Despite being a viable option for many applications, few MOFs are currently commercially available.[25] Sigma–Aldrich currently offers four MOFs from BASF: Basolite® A100, C300, F300, and Z1200, which are priced up to $28.75/g.[26] With the exception of C300, these MOFs are versions of well-known structures from the literature: Al MIL-53[27] (A100), HKUST-1,[28] or CuBTC (C300), FeBTC (F300), and ZIF-8[22] (Z1200). ZIF-8 (Z1200) is one of the most well-known chemically stable MOFs and is reportedly resistant to humid environments,[29] aqueous solutions,[30] as well as heated alkanes and other organic solvents.[22] FeBTC (F300) shows potential for separation applications,[31] but little is reported on the structure itself, except that it shows amorphous XRD behavior[32] with an empirical formula, which is not analogous to C300.[31] Two of the commercially available structures demonstrate some degree of instability during water exposure. Al MIL-53 (A100) has recently been shown to lose crystallinity and surface area upon immersion in deionized water and is reportedly less chemically stable than the Cr-analog of MIL-53.[33] After solvent removal, HKUST-1 (C300) exhibits Lewis-acid behavior via open-metal sites, which demonstrate specific benefits for selective gas adsorption[34] but is reported to degrade in the presence of water vapor.[23,29,35]

From a current literature review, it is apparent that further MOF synthesis process development is necessary to decrease the cost of manufacturing if MOFs are to compete in the adsorbent market, which is valued around $3 billion annually.[36] Most current patent literature regarding MOF synthesis applies to the use of particular ligands or metals to form families of MOFs. Other patents and patent applications

Additional Supporting Information may be found in the online version of this article.

Correspondence concerning this article should be addressed to K. S. Walton at krista.walton@chbe.gatech.edu.

cover particular applications of MOFs (e.g., liquid adsorption,[37] CO_2 separation,[38] and nano-MOFs[39]). A few others apply to nonconventional MOF synthesis techniques including microwave[40] and electrochemical.[41,42] However, to the best of our knowledge, there are no current research articles, patents, or patent applications covering the synthesis of MOFs via conventional heating in continuous-flow reactors. The design and implementation of continuous-flow MOF synthesis processes will lead to significant cost reduction and increased material production via reduced down-time.

BASF has made significant contributions to the scale-up of MOF syntheses by developing two novel methods for synthesizing MOFs[41–44] and successfully conducting the "First Industrial-Scale MOF Synthesis."[44] The electrochemical synthesis technique[41,42] patented by BASF is reportedly able to provide a continuous-flow of products via a recirculation pump with only periodic interruptions to replenish the metal anode. Alleviated safety concerns are cited as a main benefit compared to standard solvothermal synthesis techniques. Specifically, nitrate-containing metal-salts in large quantities of heated organic solvents pose a significant industrial hazard. However, many other metal-salts are used to synthesize MOFs. Also, metal anodes can be a less cost effective source of metal ions compared to their metal-salts analogs. The "solvent-free" synthesis technique[43] addresses a prominent cost and environmental concern of many MOF syntheses by forming the MOF directly in the organic acid itself, therefore eliminating the use of large quantities of solvents required for most solvothermal syntheses, which can be cost prohibitive and require additional waste disposal costs and concerns. However, certain organic ligands are difficult if not impossible to maintain in a liquid phase (e.g., terephthalic acid).[45] Despite the direct significance of these techniques, the applicability of any one synthesis method to all MOF structures is unlikely. Therefore, further development of alternative high-throughput MOF synthesis techniques is of paramount importance.

As with development of any novel material, to scale up and optimize a MOF synthesis requires a detailed understanding of the reaction kinetics as well as the characteristics of the intermediate products. Currently, a handful of articles address the determination of MOF nucleation and crystal growth rates. Kinetic data for Fe MIL-53 solvothermal syntheses are reported under conventional oven (CE), ultrasound (US), and microwave (MW) heating.[46] From XRD peak area analysis, relative crystallinity plots are used to model the crystal growth and nucleation. They report that nucleation and crystal growth rates trend as follows; US $>$ MW $>>$ CE and exhibit activation energies (E_a) for the convection oven syntheses of 39.2 and 66.4 kJ/mol for the nucleation and growth rates, respectively. Intermediate products undergo further characterization via scanning electron microscopy (SEM) and appear to be more or less uniform. Others have reported kinetic synthesis results for copper carboxylate structures, HKUST-1 and MOF-14.[47] Modeling of the *in situ* energy-dispersive X-ray diffraction (EDXRD) data also provides nucleation and growth rates for both materials and estimates the nucleation activation energies to be 71.6 and 113.9 kJ/mol for HKUST-1 and MOF-14, respectively. The higher E_{aNuc} of MOF-14 is attributed to the interpenetrated structure. The importance of synthesis time as well as temperature is demonstrated by the reported degradation of MOF-14 following prolonged exposure to synthesis conditions. Recently, the crystal growth kinetics have been reported for the water-stable Al-based MOFs, CAU-1-NH_2 and CAU-1-$(OH)_2$.[48] The materials were synthesized under microwave-assisted and standard solvothermal methods. Via EDXRD characterization, microwave-assisted syntheses reportedly decreased the crystal growth E_a of both materials slightly. Adsorption characterization was reported for the final CAU-1 products. However, these papers did not characterize the intermediate materials via adsorption testing, which can directly indicate performance differences for specific applications such as gas separation and storage and may differ vastly from the final product despite XRD congruency. A comprehensive understanding of product quality over a range of synthesis times is also vital, when considering the use of traditional flow-through crystallization reactors, which inherently have some degree of nonuniform residence time.

This work aims to develop a systematic approach to scale-up of solvothermal synthesis of UiO-66-NH_2 via convection heating. With the aforementioned benefits of water-stable and amine-functionalized MOFs, we examine the scalability of synthesis techniques within sealed vessels as well as the potential to implement a continuous-flow-through reactor. A threefold approach is used to gain insight into the optimal synthesis conditions and process design for this specific MOF. Glass and polytetrafluoroethylene (PTFE) walled vessels are used to examine nucleation site preferences. A kinetic study is conducted by collecting and characterizing intermediate synthesis products at three specific temperatures, and a continuous-flow solvothermal synthesis process is developed, which incorporates a basic draft-tube type crystallization reactor. Understanding the crystal growth behavior of specific MOFs can facilitate coupling with the well-established field of "reactive-crystallizers"[49] and provide more efficient means of commercial MOF production. We are convinced that similar iterations of this approach will prove successful for scale-up of other MOF syntheses and identification of potential pitfalls for crystallization of specific MOFs.

Experimental

Reactant solution preparation

All chemicals are procured from Sigma–Aldrich and used without any further purification. Reactant solutions containing equimolar amounts of zirconium(IV) chloride ($ZrCl_4$) and amino-terephthalic acid are dissolved in dimethyl formamide (DMF) with final concentrations identical to those reported for the parent material, UiO-66.[24] The reactant solution is stirred for $\sim$15 min or until solids are dissolved before being placed in the chosen vessels.

Reaction vessel geometry and material investigation

To examine the effect of vessel materials and geometries on UiO-66-NH_2 product quantity and quality, solvothermal syntheses are conducted in sealed borosilicate glass and PTFE-lined vessels. From visually noted MOF syntheses trends, vessel material as well as wetted surface area are expected to affect the total product yield and quality. Therefore, vessel dimensions are selected to provide a range of wetted surface area to reactant solution volume ratios (SA/V), and glass and PTFE vessels are chosen to investigate crystal growth interactions with the representative MOF synthesis vessel materials. In total, 19 sealed vessels are used including

5-, 10-, 20-, and 250-mL glass vessels as well as 23-, 46-, and 125-mL PTFE lined vessels.

An aliquot of the reactant solution described earlier is placed in each vessel, and the solution volume is recorded. All vessels are sealed, placed in a preheated isothermal convection oven, and reacted simultaneously at 393 K for the published reaction time of 24 h. After cooling, the resultant products are collected using filter paper and allowed to air-dry. The products are then weighed separately to determine a relative yield (g MOF/Vol. solution) and characterized via powder XRD (pXRD) to confirm the desired crystal phase. Brunauer, Emmett, Teller (BET) method modeling of N_2 adsorption at 77 K is conducted on the largest scale vessels for comparison to original synthesis results. This initial portion of the study provides direct insight into the UiO-66-NH_2 synthesis scalability and the resultant product characteristics.

Kinetic study

Two experiments are conducted to examine the crystal-growth reaction kinetics of the solvothermal synthesis. Ten-milliliter aliquots of the reactant solution are placed in 20-mL glass scintillation vials and arranged in three identical sand baths. The baths are then placed in separate preheated convection ovens at 373, 383, and 393 K. Every 4 h a triplet set of vials are removed from each sand bath and allowed to cool at ambient temperature. The samples are then transferred from the vials to 15-mL centrifuge tubes and centrifuged using a VanGuard V6500 centrifuge at 3400 $\pm$ 100 rpm[50] for about 10 min. The original solvent, DMF, is decanted and replaced with methanol. The centrifuging, decanting, and solvent exchange process is repeated 2 days later. The solvent-exchanged samples are allowed to air-dry uniformly and then activated in a vacuum oven for $\sim$24 h at 373 K. The activated samples are weighed under ambient conditions to understand the time and temperature dependence of the total product yield. From previous studies of UiO-66-NH_2,[23] weighing under lab ambient conditions will permit significant water vapor adsorption. Therefore, the presented yields are for relative comparison only. All samples are then characterized via pXRD, and the initial and final samples collected at each temperature are characterized by BET modeling of N_2 adsorption at 77 K.

To examine the nucleation rate and its temperature dependence, syntheses are conducted under identical conditions to those above, but samples are removed every 15 min before solvent exchange with methanol. Following previously published procedures,[46,47] nucleation rates are determined by the inverse of the synthesis time needed to produce the first Bragg XRD peak and plotted as an Arrhenius plot to predict the activation energy of nucleation, E_{aNuc}.

Continuous-flow reactor design

Stirred-sealed-vessel trials are conducted in a 20-mL scintillation vial, 250-mL glass jar, and 2-L PTFE reactor. All vessels are filled with an appropriate amount of the aforementioned reactant solution. Both the vial and the jar trials are conducted at 393 K for $\sim$24 h. The 20-mL vial synthesis utilizes a magnetic stir bar, hot plate with temperature probe, and sand bath to provide agitation and promote uniform heating. The glass jar synthesis trial is conducted by immersing the jar in a heated mineral oil bath with temperature probe. Stirring is accomplished using a magnetic stir bar and stir plate. The 2-L PTFE reactor is manufactured from a 6-in. PTFE bar, and the stirred-sealed synthesis trial is conducted with only a pressure-relief valve installed, and no inlet or outlet. The vessel is filled with $\sim$1.8 L of reactant solution and sealed by clamping between two aluminum plates. Thermal energy is provided via a drum heater and manually controlled with a variable power supply. The reactant solution temperature is monitored via infrared temperature sensor and maintained at 378–398 K for 12 h. Stirring is accomplished using a large magnetic stir bar and stir plate. The effects of dynamic synthesis conditions on the UiO-66-NH_2 production are examined via pXRD and BET modeling of the N_2 adsorption.

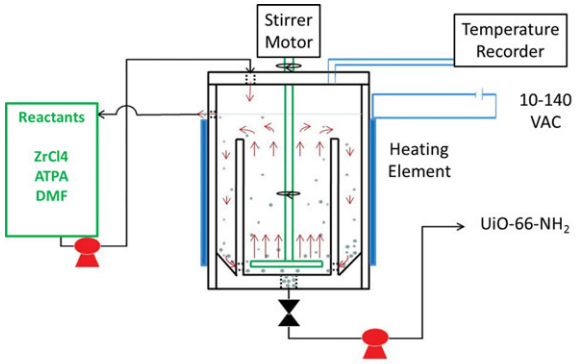

"Continuous-Flow Metal-Organic Framework Crystallization Reactor." *GTRC ID 5970*

Figure 1. Preliminary PFD of the proposed DTB crystallizer-based MOF synthesis process GTRC ID 5907 Provisional Patent Application: 61/616,746.

[Color figure can be viewed in the online issue, which is available at wileyonlinelibrary.com.]

As final proof of the concept presented in invention disclosure GTRC ID 5970 (Provisional Patent Application: 61/616,746) illustrated in Figure 1, "Continuous-flow MOF crystallization reactor," the inlet and outlet are drilled and tapped in the 2-L PTFE vessel and a 3-in. concentric PTFE tube with $^1/_4$-in. holes near the base is added to form a rudimentary draft-tube baffled (DTB) crystallization reactor. Due to materials compatibility concerns $^1/_4$-in. perfluoroalkoxy tubing and tube fittings from Swagelok® are utilized throughout the process. The aforementioned drum heater and power supply are again used for heating the continuous-flow crystallization trial. Stir bar agitation is abandoned for an overhead mixer and PTFE coated impeller to provide upward-directed axial flow within the draft-tube with the intent of selectively recirculating the small crystals and mother liquor. The temperature is recorded every 5 min via an Extech EasyView 15 Datalogger connected to a Raytech® CI1A infrared temperature sensor with air-purge collar. The reaction vessel is filled with $\sim$2 L of reactant solution and heated to 373–393 K for 12 h before flow commences. Then, the inlet from a glass reactant mixing tank containing the reactant solution is opened and the flowrate is set to about 3 mL/min with a calibrated Cole Parmer Masterflex® peristaltic pump equipped with PTFE tubing. Overflow from the reactor is recycled to the reactant mixing tank as a form of level control, reactant tank heating, and source of MOF seed crystals, which may promote a more rapid nucleation rate. The product flow is also initiated and maintained via an identical peristaltic pump at $\sim$2.8 mL/min to maintain an

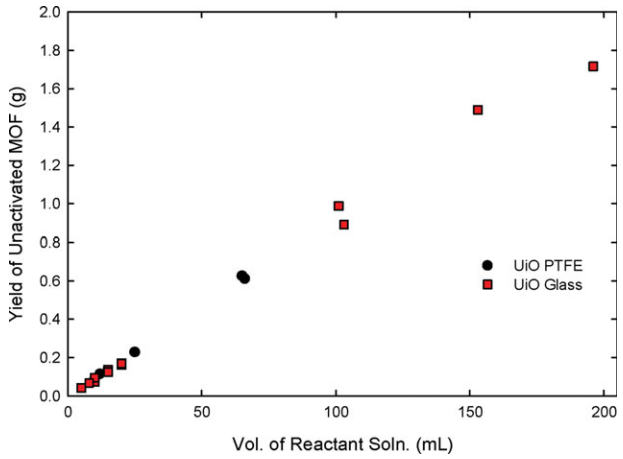

Figure 2. Plot of UiO-66-NH_2 yield illustrating direct proportionality to volume of reactant solution.

[Color figure can be viewed in the online issue, which is available at wileyonlinelibrary.com.]

average retention time (τ) of ~12 h and about 7% overflow to feed ratio. The total product is collected in a large vessel, and intermediate samples are collected directly from the outlet line every 6 h, 0.5τ. The synthesis commences under flowing conditions for 36 h or 3τ following the initial "priming" of the reactor. pXRD patterns are measured for the total bulk product, intermediate samples, and the product retained in the DTB crystallizer upon synthesis completion. Surface area modeling of N_2 adsorption at 77 K is reported for the total bulk product and the UiO-66-NH_2 retained within the crystallizer itself. Further optimization and intermediate product characterization are the subjects of ongoing research in our group.

Characterization

All powder X-ray diffractograms were collected using a PANalytical X-ray Diffractometer. For samples less than 100 mg, the MOF sample was suspended in methanol, and a few drops of the solution were placed on a low-background sample holder. Larger samples were placed in standard pXRD trays. Nitrogen adsorption measurements were performed using a Quadrasorb SI volumetric analyzer manufactured by Quantachrome Instruments. Adsorption isotherms were measured at 77 K over the range of relative pressures from 10^{-6} to 0.995 using high-purity nitrogen of 99.998% from Airgas, and the amount adsorbed was determined as a function of the equilibrium pressure. Prior to each adsorption measurement, the sample was outgassed via a FloVac Degasser for ~16 h at 473 K and under dynamic vacuum.

Results and Discussion

Reaction vessel geometry and material investigation

The results of the reaction vessel material investigation are illustrated in Figure 2. The strong linear correlation between yield of UiO-66-NH_2 and reactant solution volume (R^2 = 0.995) confirms that the crystallization reaction is directly scalable under the conditions examined, which is a nontrivial first step in MOF synthesis process design. The largest sample consists of 200 mL of reactant solution in a 250-mL glass jar, and the smallest sample is 1 mL of solution in a 5-mL vial. So, scalability is confirmed over more than two orders of magnitude. Figure 2 also illustrates that yield is not dependent on vessel material when considering PTFE and glass vessels. However, this conclusion is drawn from solely a yield basis and does not demonstrate how the hydrophobic and hydrophilic behavior of the PTFE and borosilicate glass vessels, respectively, may influence the nucleation and crystal growth mechanics. The reaction vessel geometry experimental results are illustrated in Figure S1, Supporting Information. The yield of UiO-66-NH_2 appears to be independent of the wetted surface area to reactant solution volume ratio for both PTFE and glass vessels. Therefore, nucleation and growth appear to take place primarily in the reactant solution itself. Increasing vessel volume is apparently the only means for increasing the reaction output for this specific MOF under the tested batch-style conditions.

Kinetic study

Figure 3a shows the normalized yield of UiO-66-NH_2 as a function of time at 373, 383, and 393 K. The points and error bars represent the mean and 95% confidence interval of the triplet samples, respectively. The trials all appear to asymptote to the same maximum of ~2.6 g MOF/L solution. In comparison to the originally published synthesis conditions of the parent UiO-66, which are 393 K for 24 h, we note a 67% decrease in the reaction time required to reach the maximum product yield at the same temperature. The

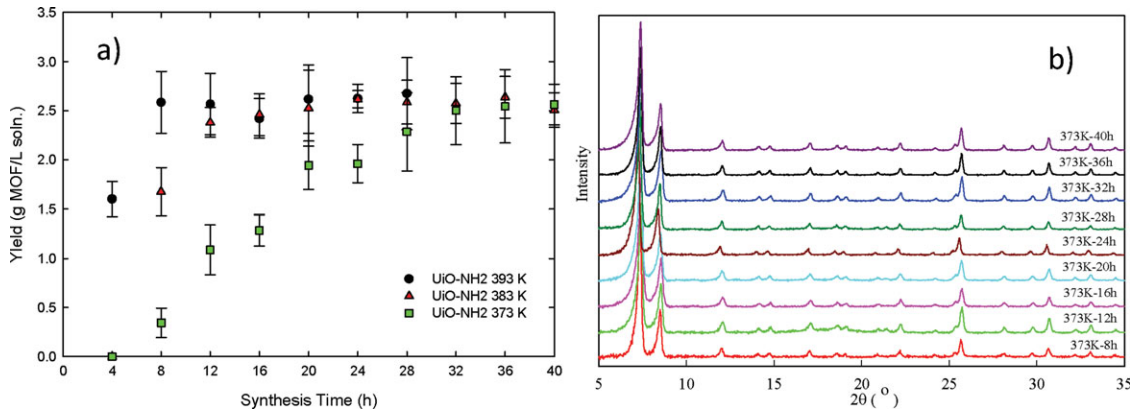

Figure 3. (a) UiO-66-NH_2 yield from triplicate samples collected every 4 h at 373, 383, and 393 K; (b) pXRD comparison of 373 K samples.

[Color figure can be viewed in the online issue, which is available at wileyonlinelibrary.com.]

Table 1. BET Surface Areas (m^2/g) of UiO-66-NH_2 Synthesis Products at 373, 383, and 393 K

	373 K	383 K	393 K
Min. time	1070 (8)	947 (8)	1000 (4)
Max. time	855 (40)	1010 (40)	1010 (28)

BET surface areas (m^2/g) from N2 adsorption at 77 K. Min. and Max. times are the shortest and longest times, respectively, at which an appropriate amount of product was obtained for adsorption testing. The values given in parentheses are time taken (in hours) for the respective synthesis.

24-h original synthesis time was likely chosen for convenience. However, the difference amounts to a significant increase in throughput from a process vantage point. Figure 3b illustrates the pXRD diffractograms collected for the 393 K synthesis products. Under all temperatures examined and for all samples collected, we do not note any discernible differences in pXRD patterns, which are consistent with those of the desired product, UiO-66-NH_2. Each triplet of samples is then combined, and further structure confirmation is accomplished via BET modeling of the N_2 adsorption at 77 K. Table 1 shows the resultant BET surface areas of the initial and final samples at each synthesis temperature, which are relatively consistent except for the 373 K, 40 h sample, which is about 15% lower than the final samples at 383 and 393 K. An independent 373 K 40 h trial is generated to confirm the lower BET surface area, yielding 867 m^2/g, which is within 1.4% of the first trial. The reduced BET surface area of the 373 K, 40 h sample may be a result of larger crystal formation or more tightly packed agglomerates, which may form under longer synthesis times and reduce the BET surface area contributions from the geometric properties of the crystal particles themselves. This reasoning would be directly congruent with the idea patented by UOP[39] concerning the synthesis of MOF nanoparticles with higher effective surface areas. However, the yield, pXRD, and N_2 adsorption results still demonstrate that there are multiple temperatures and synthesis times capable of producing UiO-66-NH_2 with nearly identical performance characteristics. From a flow-through reactor design viewpoint, this is highly advantageous and is reportedly not the case for some MOFs.[47]

An example of the XRD diffractograms used to identify the time at which nucleation occurs at 373 K and the resultant nucleation rate are shown in Figure 4a. The resultant Arrhenius plot is produced by comparing the nucleation rates determined at 373, 383, and 393 K (Figure 4b). The activation energy of UiO-66-NH_2 nucleation (E_{aNuc}) predicted by the Arrhenius plot is ~64.5 kJ/mol. A higher value compared to the E_{aNuc} reported for Fe MIL-53, 39.2 kJ/mol,[46] may be indicative of the difference in coordination environments. UiO-66-NH_2 consists of highly coordinated clusters, which form an eight-coordinated state when hydrated and seven-coordinated upon dehydroxylation,[24,51] requiring a higher E_a to facilitate nucleation compared to the four-coordinated Fe MIL-53 framework.[52] Furthermore, the E_{aNuc} for UiO-66-NH_2 is still significantly lower than that of MOF-14, which is 113.9 kJ/mol for convection oven synthesis and is expected to be relatively high as an attribute of the framework interpenetration.[47] HKUST-1 E_{aNuc} of 71.6 kJ/mol[47] is within 11% of the value predicted for UiO-66-NH_2. The nucleation rates and predicted E_{aNuc} for UiO-66-NH_2 solvothermal synthesis are congruent with reported values for other MOFs, which not only validate our findings but also predict that UiO-66-NH_2 continuous-flow crystallization may be representative of a typical MOF crystallization process. Crystal size distribution, a common figure of merit for crystal growth kinetics, is not examined in this work. From a fixed-bed adsorption perspective, the ability to press pellets without affecting the structure[24] diminishes the need to control MOF particle size. Also, UiO-66 crystallites are typically submicron,[24] suggesting that the main dominant mechanism is nucleation.

Continuous-flow reactor design

The pXRD comparisons of the stirred-sealed synthesis trials are presented in Figure 5. From peak position comparison, all diffractograms appear to have consistent crystallinity as UiO-66-NH_2. The difference in relative peak heights for the stirred-PTFE reactor compared to the other trials is attributed to pXRD sample and sample pan size differences. More specifically, the 2-L PTFE reactor provides a sample approximately two orders of magnitude larger than the 20-mL vial, and a larger XRD sample pan is selected to accurately examine the cumulative sample. BET modeling of the N_2 adsorption at 77 K predicts effective surface areas of 630, 680, and 830 m^2/g for the 20-mL vial, 250-mL jar, and

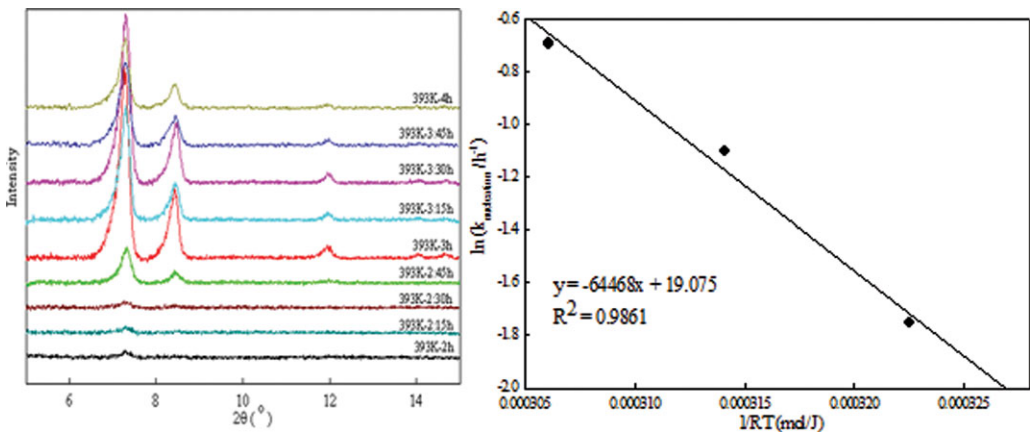

Figure 4. (a) UiO-66-NH_2 pXRD used to determine nucleation rate (393 K); and (b) Arrhenius plot of experimentally determined nucleation rates.

[Color figure can be viewed in the online issue, which is available at wileyonlinelibrary.com.]

2-L PTFE reactor, respectively. The surprising increase of surface area with increasing reaction vessel volume may be attributed to more accurate temperature control during the 2 L PTFE trial, in which the solution temperature itself is monitored with an infrared temperature sensor. The temperatures of the jar and vial trials are monitored by placing the hot plate probe in the oil and sand baths, respectively, instead of the actual reactant solution. Fluid dynamics within the vessel may also influence the stirred-trial product quality. Assuming the fluid properties themselves are constant for all three stirred-sealed trials, the Reynolds numbers cover a 12-fold range of values presented in Table S1, Supporting Information, which will need to be investigated in more detail to predict any specific relationship between fluid dynamics and MOF product quality. However, the trend is in agreement with the claim of UOP's patent application[39] for nano-MOF synthesis, which utilizes agitation to decrease particle size as well as agglomeration and increase the resultant effective surface area. The stirred trial BET results are notably lower than the initial 20-mL vial synthesis conducted under static conditions. However, we note a similar decrease in surface area during the characterization of the larger samples collected during the reaction vessel geometry and material investigation. The largest volume sample of the scale-up synthesis work consists of 200 mL of reactant solution in a 250-mL glass jar, which yields a BET surface area of 810 m^2/g. In general, commercially available MOFs do not tend to have high degrees of precision associated with their BET surface areas (e.g., C300 from Sigma–Aldrich via BASF is reported to have BET surface areas from 1500 to 2100 m^2/g or 1800 $m^2/g \pm 17\%$),[53] and the benefits of the proposed flow-through synthesis process may far outweigh any moderate reduction in surface area. Other studies conducted in our lab (Figure S4, Supporting Information) demonstrate how differences in BET surface areas of up to 25% for the same MOF result in very little difference in the adsorption behavior for carbon dioxide, especially at low pressure.

Figure 6 illustrates the pXRD of the bulk product collected from the continuous-flow synthesis trial as well as the product retained within the crystallizer following the synthesis trial. pXRD of the intermediate samples are shown in Figure S7, Supporting Information, and illustrate peak position and intensity agreement confirming formation of the desired product, UiO-66-NH_2. The BET surface areas of the bulk product and product from within the reactor are 530 and 640 m^2/g, respectively. Drastic reduction of surface area, which is a direct measure of product quality for many MOF applications, may be indicative of insufficient or non-uniform retention time or significant impurity concentration. However, we see relatively similar product quality with a 22% loss from the stirred-batch trial in the same reaction vessel. These novel results directly demonstrate the feasibility of continuous-flow MOF synthesis. Further optimization will be conducted in our lab to optimize crystalline-product yield and quality. However, these results are still of principal importance to the industrial scale-up of MOFs and subsequent transition to potential applications.

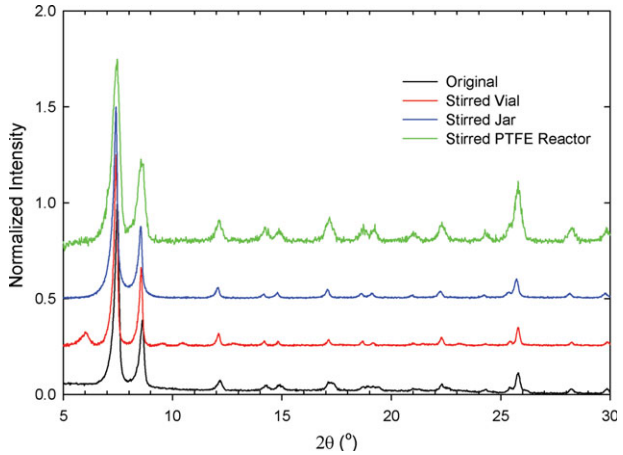

Figure 5. pXRD of stirred-sealed synthesis trials.

Intensities are normalized to account for the differences in sample and sample pan sizes. [Color figure can be viewed in the online issue, which is available at wileyonlinelibrary.com.]

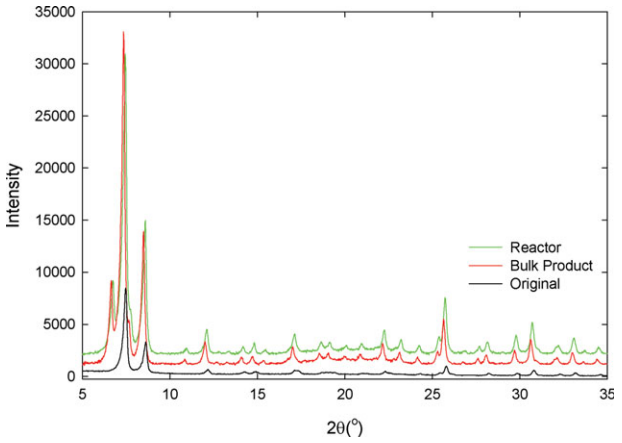

Figure 6. pXRD of the "Bulk Product" from the flow-through synthesis trial and the material retained within the DTB crystallization "Reactor" compared with original UiO-66-NH_2 sample.

[Color figure can be viewed in the online issue, which is available at wileyonlinelibrary.com.]

Conclusions

In summary, we have developed and implemented a methodical approach to the scale-up synthesis of UiO-66-NH_2 and presented initial proof of concept results for a novel continuous-flow MOF synthesis process, which implements a flow-through crystallization reactor. During batch-style syntheses, we find that crystal yield is directly proportional to the volume of reactant solution in the vessel and independent of the wetted surface area to volume ratio. The yield also shows no preference for PTFE or borosilicate glass vessels. Collecting intermediate products during the sealed solvothermal syntheses at three temperatures illustrates the bulk reaction kinetics. We find that the maximum yield is reached at all three temperatures, and at the originally published synthesis temperature, we are able to obtain the maximum yield with a 67% decrease in reaction time. Relatively uniform product quality is noted from the first collectable product to the final product and is illustrated via pXRD and BET surface area comparison. The intermediate products are also characterized via pXRD, and nucleation rates are determined at each temperature. We find the nucleation rates follow the Arrhenius equation and predict a E_{aNuc} of 64.5 kJ/mol,

which is in the range reported for other MOFs and appears to be representative of the highly coordinated Zr-MOF structure. Stirred-synthesis trials are conducted over a 100-fold range of reaction vessel volumes, and all products are compared via pXRD and BET modeling of the N_2 adsorption at 77 K. A novel continuous-flow MOF crystallization process is reported. Resultant pXRD of intermediate products show some intensity variance, which is likely attributed to accumulation of crystalline product within the reactor and lower concentration of MOF in the product stream. However, the bulk product is in good agreement with the pXRD found for the original UiO-66-NH_2 product, and BET surface area of the product retained within the reactor is within 22% of the 827 m^2/g found for the stirred-batch trial in the same vessel. Further optimization of the process is necessary to produce a more consistent concentration of MOF product. However, the importance of the novel crystallization method cannot be overstated. The reduction in down-time and increased throughput can directly aid in the transition of MOFs from the lab to an applied level.

Acknowledgments

This material is based on work supported by the Army Research Office under contract W911NF-10-1-0076.

Literature Cited

1. Glover TG, Peterson GW, Schindler BJ, Brittand D, Yaghi O. MOF-74 building unit has a direct impact on toxic gas adsorption. *Chem Eng Sci*. 2010;66(2):163–170.
2. Liu J, Benin AI, Furtado AMB, Jakubczak P, Willis RR, LeVan MD. Stability effects on CO(2) adsorption for the DOBDC series of metal-organic frameworks. *Langmuir*. 2011;27(18):11451–11456.
3. Karra JR, Walton KS. Molecular simulations and experimental studies of CO_2, CO, and N-2 adsorption in metal-organic frameworks. *J Phys Chem C*. 2010;114(37):15735–15740.
4. Mu B, Schoenecker PM, Walton KS. Gas adsorption study on mesoporous metal-organic framework UMCM-1. *J Phys Chem C*. 2010;114(14):6464–6471.
5. Millward AR, Yaghi OM. Metal-organic frameworks with exceptionally high capacity for storage of carbon dioxide at room temperature. *J Am Chem Soc*. 2005;127(51):17998–17999.
6. Wang C, Xie ZG, deKrafft KE, Lin WL. Doping metal-organic frameworks for water oxidation, carbon dioxide reduction, and organic photocatalysis. *J Am Chem Soc*. 2011;133(34):13445–13454.
7. Tanabe KK, Cohen SM. Engineering a metal-organic framework catalyst by using postsynthetic modification. *Angew Chem Int Ed Engl*. 2009;48(40):7424–7427.
8. Horcajada P, Serre C, Ferey G, Couvreur P, Gref R. Porous materials, loading and release of antitumural and antiretroviral drugs. *Actual Chim*. 2011; (348–349):58–63.
9. McKinlay AC, Morris RE, Horcajada P, Ferey G, Gref R, Couvreur P, Serre C. BioMOFs: metal-organic frameworks for biological and medical applications. *Angew Chem Int Ed Engl*. 2010;49(36):6260–6266.
10. Miller SR, Heurtaux D, Baati T, Horcajada P, Greneche JM, Serre C. Biodegradable therapeutic MOFs for the delivery of bioactive molecules. *Chem Commun*. 2010;46(25):4526–4528.
11. Zacher D, Shekhah O, Woll C, Fischer RA. Thin films of metal-organic frameworks. *Chem Soc Rev*. 2009;38(5):1418–1429.
12. Shekhah O, Liu J, Fischer RA, Woll C. MOF thin films: existing and future applications. *Chem Soc Rev*. 2011;40(2):1081–1106.
13. Demessence A, D'Alessandro DM, Foo ML, Long JR. Strong CO_2 binding in a water-stable, triazolate-bridged metal-organic framework functionalized with ethylenediamine. *J Am Chem Soc*. 2009;131(25):8784–8786.
14. Nguyen JG, Tanabe KK, Cohen SM. Postsynthetic diazeniumdiolate formation and NO release from MOFs. *Crystengcomm*. 2010;12(8):2335–2338.
15. Wang ZQ, Tanabe KK, Cohen SM. Tuning hydrogen sorption properties of metal-organic frameworks by postsynthetic covalent modification. *Chem Eur J*. 2010;16(1):212–217.
16. Garibay SJ, Cohen SM. Isoreticular synthesis and modification of frameworks with the UiO-66 topology. *Chem Commun*. 2010;46(41):7700–7702.
17. Kaye SS, Dailly A, Yaghi OM, Long JR. Impact of preparation and handling on the hydrogen storage properties of Zn4O(1,4-benzenedicarboxylate)(3) (MOF-5). *J Am Chem Soc*. 2007;129(46):14176–14177.
18. Wu TJ, Shen LJ, Luebbers M, Hu CH, Chen QM, Ni Z, Masel, RI. Enhancing the stability of metal-organic frameworks in humid air by incorporating water repellent functional groups. *Chem Commun*. 2010;46(33):6120–6122.
19. Hausdorf S, Wagler J, Mossig R, Mertens F. Proton and water activity-controlled structure formation in zinc carboxylate-based metal organic frameworks. *J Phys Chem A*. 2008;112(33):7567–7576.
20. Greathouse JA, Allendorf MD. The interaction of water with MOF-5 simulated by molecular dynamics. *J Am Chem Soc*. 2006;128(33):10678–10679.
21. Choi HJ, Dinca M, Dailly A, Long JR. Hydrogen storage in water-stable metal-organic frameworks incorporating 1,3-and 1,4-benzenedipyrazolate. *Energy Environ Sci*. 2010;3(1):117–123.
22. Park KS, Ni Z, Cote AP, Choi JY, Huang RD, Uribe-Romo FJ, Chae HK, O'Keeffe M, Yaghi OM. Exceptional chemical and thermal stability of zeolitic imidazolate frameworks. *Proc Natl Acad Sci USA*. 2006;103(27):10186–10191.
23. Schoenecker PM, Carson CG, Jasjuja H, Flemming CJJ, Walton KS. Effect of water adsorption on retention of structure and surface area of metal-organic frameworks. *Ind Eng Chem Res*. 2012;51(18):6513–6519.
24. Cavka JH, Jakobsen S, Olsbye U, Guillou N, Lamberti C, Bordiga S, Lillerud KP. A new zirconium inorganic building brick forming metal organic frameworks with exceptional stability. *J Am Chem Soc*. 2008;130(42):13850–13851.
25. Ferey G. Some suggested perspectives for multifunctional hybrid porous solids. *Dalton Trans*. 2009:4400–4415.
26. Basolite®Pricing. Sigma–Aldrich. Available at: http://www.sigmaaldrich.com/catalog/product/aldrich/691348 (Accessed May 14, 2012).
27. Loiseau T, Serre C, Huguenard C, Fink G, Taulelle F, Henry M, Bataille T, Ferey G. A rationale for the large breathing of the porous aluminum terephthalate (MIL-53) upon hydration. *Chem-Eur J*. 2004;10(6):1373–1382.
28. Chui SSY, Lo SMF, Charmant JPH, Orpen AG, Williams ID. A chemically functionalizable nanoporous material Cu-3(TMA)(2)(H2O)(3) (n). *Science*. 1999;283(5405):1148–1150.
29. Kusgens P, Rose M, Senkovska I, Frode H, Henshel A, Siegle S, Kaskel S. Characterization of metal-organic frameworks by water adsorption. *Microporous Mesoporous Mater*. 2009;120(3):325–330.
30. Ge D, Lee HK. Water stability of zeolite imidazolate framework 8 and application to porous membrane-protected micro-solid-phase extraction of polycyclic aromatic hydrocarbons from environmental water samples. *J Chromatogr A*. 2011;1218(47):8490–8495.
31. Centrone A, Santiso EE, Hatton TA. Separation of chemical reaction intermediates by metal-organic frameworks. *Small*. 2011;7(16):2356–2364.
32. Babu KF, Kulandainathan MA, Katsounaros I, Rassaei L, Burrows AD, Raithby PR, Marken F. Electrocatalytic activity of Basolite (TM) F300 metal-organic-framework structures. *Electrochem Commun*. 2010;12(5):632–635.
33. Kang IJ, Khan NA, Haque E, Jhung SH. Chemical and thermal stability of isotypic metal-organic frameworks: effect of metal ions. *Chem-Eur J*. 2011;17(23):6437–6442.
34. Liu J, Wang Y, Benin AI, Jakubczak P, Willis RR, LeVan MD. CO_2/H_2O Adsorption equilibrium and rates on metal-organic frameworks: HKUST-1 and Ni/DOBDC. *Langmuir*. 2010;26(17):14301–14307.
35. Low JJ, Benin AI, Jakubczak P, Abrahamian JF, Faheem SA, Willis RR. Virtual high throughput screening confirmed experimentally: porous coordination polymer hydration. *J Am Chem Soc*. 2009;131(43):15834–15842.
36. Cychosz KA, Ahmad R, Matzger AJ. Liquid phase separations by crystalline microporous coordination polymers. *Chem Sci*. 2010;1(3):293–302.
37. Muller U, Hesse M, Putter H. Liquid absorption by metal-organic frameworks. United States Patent Application Publication. 2009;7534303.
38. Schubert M, Muller U, Kiener C. Method for the separation of carbon dioxide using a porous metal-organic framework. United States Patent Publication. 2009;7,556,673.

39. Benin A, Willis RR. Synthesis methodology to produce nano metal organic framework crystals. United States Patent Application Publication. 2012;US 2012/00033475 A1.
40. Ni Z, Masel RI. Rapid metal organic framework molecule synthesis method. United States Patent Application Publication. 2009;11/785, 102.
41. Muller U, Putter H, Hesse M, Schuber M, Wessel H, Huff J, Guzmann M. Method for electrochemical production of a crystalline porous metal organic skeleton material. United States Patent Application Publication. 2004;10/580,407.
42. Mueller U, Schubert M, Teich F, Puetter H, Schierle-Arndt K, Pastre J. Metal-organic frameworks—prospective industrial applications. *J Mater Chem*. 2006;16(7):626–636.
43. Leung E, Muller U, Cox G. Solvent-free preparation of magnesium formate-based porous metal-organic framework. United States Patent Application Publication. 2012;US 2012/0016160 A1.
44. Kummeter M. First Industrial-Scale MOF Synthesis. Available at: http://www.basf.com/group/pressrelease/P-10-428 (Accessed May 14, 2012).
45. Lucchesi CA, Lewis WT. Latent heat of sublimation of terephthalic acid from differential thermal analysis data. *J Chem Eng Data*. 1968;13(3):389–391.
46. Haque E, Khan NA, Park JH, Jhung SH. Synthesis of a metal-organic framework material, iron terephthalate, by ultrasound, microwave, and conventional electric heating: a kinetic study. *Chem-Eur J*. 2010;16(3):1046–1052.
47. Millange F, El Osta R, Medina ME, Walton RI. A time-resolved diffraction study of a window of stability in the synthesis of a copper carboxylate metal-organic framework. *Crystengcomm*. 2011;13(1): 103–108.
48. Ahnfeldt T, Moellmer J, Guillerm V, Staudt R, Serre C, Stock N. High-throughput and time-resolved energy-dispersive X-ray diffraction (edxrd) study of the formation of CAU-1-(OH)(2): microwave and conventional heating. *Chem-Eur J*. 2011;17(23):6462–6468.
49. Myerson AS. *Handbook of Industrial Crystallization*, 2nd ed. Woburn, MA: Butterworth-Heinemann, 2002.
50. Vanguard V6500 centrifuge. SCSI & Fiber Optic Connectivity Solutions. Available at: http://www.cecocablingsystems.com/centrifuge.htm. (Accessed May 14, 2012).
51. Valenzano L, Civalleri B, Chavan S, Bordiga S, Nilsen NH, Jakobsen S, Lillerud KP, Lamberti C. Disclosing the complex structure of UiO-66 metal organic framework: a synergic combination of experiment and theory. *Chem Mater*. 2011;23(7):1700–1718.
52. Millange F, Serre C, Ferey G. Synthesis, structure determination and properties of MIL-53 as and MIL-53ht: the first Cr-III hybrid inorganic–organic microporous solids: Cr-III(OH)·{O_2C-C_6H_4-CO_2}·{HO_2C-C_6H_4-CO_2H}(x). *Chem Commun*. 2002;(8):822–823.
53. The world record in surface area BASOLITE metal organic frameworks. Available at: http://www.sigmaaldrich.com/etc/medialib/docs/Aldrich/General_Information/basf_basolite_handout_051908.-Par.0001.File.tmp/basf_basolite_handout_051908.pdf (Accessed on May 14, 2012).

Manuscript received May 31, 2012, and revision received July 20, 2012.